Surface Characterization of Poly(acrylonitrile) Membranes Graft-Polymerized with Ionic Monomers As Revealed by ζ Potential Measurement

Toshihiko Jimbo,[†] Mitsuru Higa,[‡] Norihiko Minoura,[§] and Akihiko Tanioka*,[†]

Department of Organic and Polymeric Materials, Tokyo Institute of Technology, 2-12-1 Ookayama, Meguro-ku, Tokyo 152-8552, Japan, Department of Applied Chemistry and Chemical Engineering, Yamaguchi University, 2557 Tokiwadai, Ube-shi, Yamaguchi 755-8611, Japan, and National Institute of Materials and Chemical Research, 1-1 Higashi, Tsukuba-shi, Ibaraki 305-8565, Japan

Received May 16, 1997; Revised Manuscript Received November 10, 1997

ABSTRACT: Anionic and cationic monomers were graft-polymerized onto poly(acrylonitrile) (PAN) membrane surfaces. The graft polymerization was initiated by an oxidation−reduction system at 25 °C. Grafted PAN membrane surfaces yielded FT-IR/ATR spectra clearly different from that of an unmodified PAN membrane, because of the presence of the graft chains. ζ potentials of the pore surfaces of the grafted PAN membranes were obtained from streaming potential measurements. The surface properties are discussed with respect to a single site dissociation model, which is based on the protonation and deprotonation of charged surface groups. In this study, we obtained some characteristic parameters of the pore surfaces from the theoretical fits using the site dissociation model. This approach gives direct insight into the pore surface properties of the membrane. The results could be well explained by an ion-pairing effect in terms of different charge characteristics between membranes having hydrophobic or hydrophilic graft chains: charge groups of hydrophobic graft chains are likely to form ion pairs with counterions from the external solution. The local dielectric constant surrounding ion pairs plays an important role in the surface effective charge concentration.

1. Introduction

Synthetic polymer membranes and films have been modified by many researchers by grafting with various kinds of functional monomers to improve their hydrophilic performance.[1−11] Hydrophilic surfaces have attracted much attention in the field of biomedical materials related to the interaction between polymeric surfaces and proteins or cells. So far, many studies have been devoted to surface−protein interactions in the conformational changes of proteins,[12] modeling of protein adsorption,[13] and adsorption kinetics of proteins onto a substrate.[14,15] However, processes affecting the states of surface charge such as polarity, charge amount, and charge species have not yet been extensively studied in connection with protein adsorption phenomena; many aspects of such processes remain unclear. Protein adsorption can be affected not only by surface charge but also by porosity and surface roughness.[16] Membrane fouling due to adsorption of charged particles degrades membrane properties drastically. Therefore, it is important to minimize such adsorption on membrane surfaces to obtain excellent performance in applications such as protein or blood filtration and artificial kidneys. To interpret these very complicated protein adsorption phenomena, a more detailed characterization of the surface of membrane pores is necessary, especially one focusing on the state of surface charge.

In many cases, graft polymerization is induced by the radicals produced by plasma treatment,[7−10] UV irradiation,[3,4,11] and thermal decomposition of peroxide;[1,2] initiation by an oxidation−reduction system (redox system) is an effective method capable of inducing grafting even at relatively low temperatures.[5,6,17] There are many reports of experimental and kinetic establishment of redox polymerization. We introduced the redox system for initiation of graft polymerization onto a poly(acrylonitrile) (PAN) membrane at 25 °C to ensure that the structure of the grafted membrane would be largely unaltered; grafting using heat induces structural deformation. Poly(acrylonitrile) (PAN), used in this study, is a suitable material to modify: various charge groups can be easily added to the PAN substrate via hydrolysis of −C≡N groups,[5,18,19] treatment with hydroxylamine,[5,6] and grafting with ionic monomers,[1,3−6] and the material shows good mechanical properties for membrane use. We prepared PAN membranes and subsequently grafted some ionic monomers, (methacryloxy)ethyl phosphate (MOEP), acrylic acid (AAc), 2-(diethylamino)ethyl methacrylate (DEAEM), and [(*N*,*N*-(dimethylamino)propyl]-acrylamide (DMAPAA), onto the membrane surfaces. We selected these monomers to examine the effects of surface charge not only on polarity but also on surface hydrophobicity and hydrophilicity.

It is very difficult to characterize the surfaces of porous materials in aqueous media, because analytical methods are limited. However, electrokinetic characterizations[11,20−29] by means of streaming potential and electroosmosis can be more useful for surface analysis of porous substrates, films, and fibers than conventional X-ray diffraction (XRD), infrared spectroscopy (IR), contact angle measurement, and X-ray photoelectron spectroscopy (XPS). The ζ potential is the potential between a pore surface and the shear plane; it is generated by hydrodynamic flow induced by a pressure difference across a membrane. We calculated the ζ

* Tel: +81-3-5734-2426. Fax: +81-3-5734-2876. E-mail: atanioka@o.cc.titech.ac.jp.
[†] Tokyo Institute of Technology.
[‡] Yamaguchi University.
[§] National Institute of Materials and Chemical Research.

S0024-9297(97)00692-X CCC: $15.00
Published on Web 02/03/1998

potential from observed streaming potentials to obtain information related to the surface charge of the pores. Electrokinetic measurements have been theoretically established and widely utilized for pursuing adsorption phenomena of macromolecules onto substrates;[23] these measurements are also sensitive to the pH dependence of dissociation of the charged surface groups.[26,27,30] Healy and White[29,31] have suggested that surface charge can be described in terms of a site dissociation model for surface ionizable groups. Their model seems to be an effective procedure to describe pore surface properties in detail; surface characteristic parameters such as surface charge density, dissociation constant, and isoelectric point are ascribed great importance for interpretation of native surface properties with respect to protein adsorption phenomena. We discuss our results with respect to ion-pairing effects, which have been suggested by Mafé et al.[32] as an approach to describe the effective charge concentration in ion exchange membranes with low dielectric constant region. We explore the hydrophilic and hydrophobic effects of the graft chains by calculating the ion-pairing effects to clarify the states of the pore surface charge for the grafted PAN membranes, thus taking into account the local dielectric constant surrounding the ion pairs.

2. Experimental Section

2.1. Membranes. 2.1.1. Materials. Poly(acrylonitrile) (PAN) powder (M_w = 130 000) was provided by Mitsubishi Rayon Co., Ltd., Japan. Poly(vinylpyrrolidone) (PVP), *N*,*N*-dimethylformamide (DMF), ferrous sulfate, hydrogen peroxide, sodium bisulfite, and ammonium persulfate were purchased from Wako Pure Chemical Co., Ltd., Japan. These reagents were of extra-pure grade and were used without further purification. Acrylic acid (AAc) (Wako Pure Chemical Co., Ltd., Japan), (methacryloxy)ethyl phosphate (MOEP) (Johoku Chemical Co., Ltd., Japan), 2-(diethylamino)ethyl methacrylate (DEAEM) (Aldrich Chemical Co., Inc.), and [(*N*,*N*-(dimethylamino)propyl]acrylamide (DMAPAA) (Kohjin Co., Ltd., Japan) were used as monomers for grafting (chemical structures shown in Figure 1).

2.1.2. Membrane Preparation. A mixed solution of 12.0 wt % PAN powder and 3.0 wt % PVP in DMF was stirred at 70 °C for 5 h and was subsequently cooled to 25 °C. The solution was cast onto a glass plate guided by a 150 μm thick spacer. After the solvent was evaporated for 30 s at 25 ± 1 °C and a humidity of 60 ± 2%, the plate was immersed in a coagulation medium consisting of a 40 vol % glycerol and water mixture for 20 min at 10 °C. The membrane was removed from the plate and washed with abundant deionized water for 3 days to remove PVP. The PAN membrane thus obtained had a thickness of 110 μm and a hydraulic permeability of 1200 ± 50 mL·m^{-2}·h^{-1}·cm^{-1} H_2O under a static pressure of 75.0 cm H_2O.

2.1.3. Graft Polymerization. Graft polymerization onto PAN membrane surfaces was performed by initiation of a redox system. Fifteen pieces of PAN membrane, each 5 cm × 5 cm and 110 μm thick, were immersed in 500 mL of aqueous solution containing a monomer; some of the dissolved oxygen was removed with bubbling with nitrogen gas. The monomer solution was kept in a reciprocating shaker for 1 h at 25 °C after addition of the reduction reagent; the graft polymerization was then initiated by addition of peroxide as an oxidation reagent at 25 °C. The detailed reaction conditions are shown in Table 1. Following graft polymerization, membranes were washed with abundant deionized water for 24 h at 25 °C and then sequentially with 1 mM HCl and 0.1 mM NaOH at 25 °C for 24 h each to remove the homopolymer produced simultaneously.

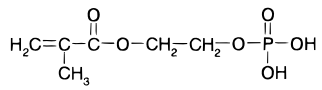

Methacryloxyethyl Phosphate (MOEP)

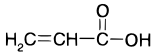

Acrylic Acid (AAc)

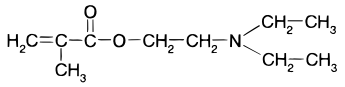

2-(Diethylamino)ethyl Methacrylate (DEAEM)

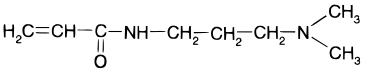

N,N-(Dimethylamino)propyl Acrylamide (DMAPAA)

Figure 1. Chemical structures of monomers to be grafted.

2.2. Measurements. 2.2.1. Hydraulic Permeability of PAN Membranes. The hydraulic permeability of the membranes was calculated from the flow rate of deionized water after elution for 20 min at 25 °C, under a constant hydrostatic pressure difference of 75.0 cm H_2O across the membrane. The membrane area exposed to the flow was 4.9 cm^2.

2.2.2. Atomic Force Microscopy (AFM). Analysis of the morphology of the top surface of freeze-dried membranes was carried out in the dry state with a model SPA-300 atomic force microscope (Seiko Instruments, Japan).

2.2.3. Fourier Transform Infrared Spectroscopy/Attenuated Total Reflection (FT-IR/ATR). FT-IR/ATR spectra were acquired with a model JIR-MICRO6000 FT-IR (JEOL, Japan) equipped with an ATR unit (KRS-5 crystal, 45 degrees, Specac, Ltd.). Dried membranes were pressed on both sides of the crystal to ensure the sensitivity of the spectra obtained. All spectra were taken by 500 scans at a nominal resolution of 4 cm^{-1}.

2.2.4. ζ Potential from Streaming Potential Measurement. The device we constructed for the streaming potential

Table 1. Reaction Conditions and Properties of Grafted PAN Membranes

sample	monomer concn (wt %)	reacn time (h)	hydraulic permeability (mL·m^{-2}·h^{-1}·cm^{-1} H_2O)[a]	pore diameter by AFM (nm)[b]	ζ potential (mV)[c]
unmodified PAN-1			1223	90.6 ± 31.2	−5.57
unmodified PAN-2			930	60.6 ± 12.6	−5.27
MOEP-*g*-PAN	2.5	2.0	691	49.7 ± 8.3	−9.08
AAc-*g*-PAN	1.0	2.0	743	51.1 ± 9.7	−18.19
DEAEM-*g*-PAN	3.0	1.0	753	48.1 ± 11.4	+3.47
DMAPAA-*g*-PAN	0.5	2.0	873	50.6 ± 8.6	+15.16

[a] Standard deviation is within 7%. [b] Determined from AFM according to the method of ref 34. The values are indicated by mean ± S.D. of eight points. [c] Values at pH = 5.45.

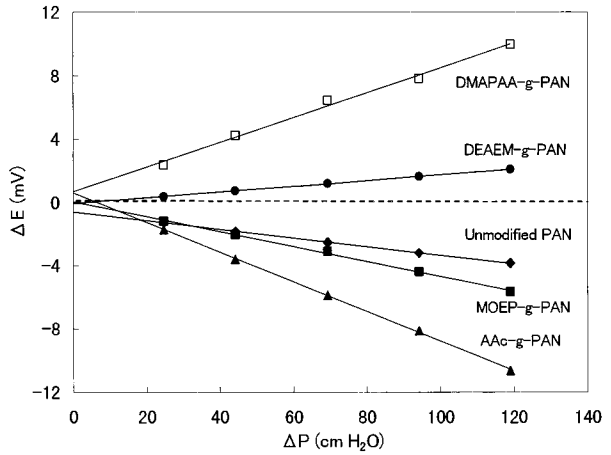

Figure 2. Dependence of streaming potential on pressure difference for grafted PAN membranes used in this study (1 mM KCl, pH 5.45).

measurements was of a type similar to that previously described.[33] The membrane was precisely attached between the two 64 cm^3 compartments to prevent liquid leakage. Stirring was done until just before data collection. Hydrostatic pressure across the membrane was applied by changing the solution levels of both reservoirs. The membrane area exposed to the flow was 1.8 cm^2. The electrodes were made of silver/silver chloride. The streaming potential, ΔE, was measured with a digital multimeter (HP 3458A Multimeter, Yokogawa-Hewlett-Packard, Ltd.) at 25 °C and recorded with a microcomputer as a function of the pressure difference, ΔP. Good linearity between the pressure difference, ΔP, and the streaming potential, ΔE, could be obtained for all samples (Figure 2). The ζ potential was calculated from the streaming potential/pressure difference slope with the Smoluchowski−Helmholtz equation as follows:[28]

$$\frac{\Delta E}{\Delta P} = \frac{\epsilon\zeta}{\eta\lambda} \tag{1}$$

where ϵ and η are the solution permittivity and the solution viscosity, respectively, and λ is the solution conductivity. The surface charge density of the pores was calculated from the ζ potential using the Gouy−Chapman equation:[28]

$$\sigma_s = \frac{2\epsilon kT\kappa}{z_+ e}\sinh\left(\frac{z_+ e\zeta}{2kT}\right) \tag{2}$$

where k is the Boltzman constant, T the temperature, κ the reciprocal of the electrical double-layer thickness, z_+ the valency of the counterions, and e the Coulombic charge. A 1 mM KCl solution was used throughout the measurements, and solution pH was adjusted by adding 0.1 N HCl and 0.1 N KOH. The measured pH range was chosen so as to eliminate experimental error resulting from damage to the electrodes or change in ionic strength.

3. Results and Discussion

3.1. Graft Polymerization onto a PAN Membrane. Graft polymerization onto the PAN membrane was initiated by the redox system of $Fe^{II}-H_2O_2$ for an anionic monomer solution and $NaHSO_3-(NH_4)_2S_2O_8$ for a cationic monomer solution at 25 °C. Reaction conditions for the graft polymerization were chosen so as to have the same pore morphology for each membrane to ensure well-defined grafted PAN membranes in which the ζ potential would be dependent on the pore morphology. The detailed membrane characteristics and reaction conditions are shown in Table 1. "Unmodified PAN-1" was the original membrane used for the graft

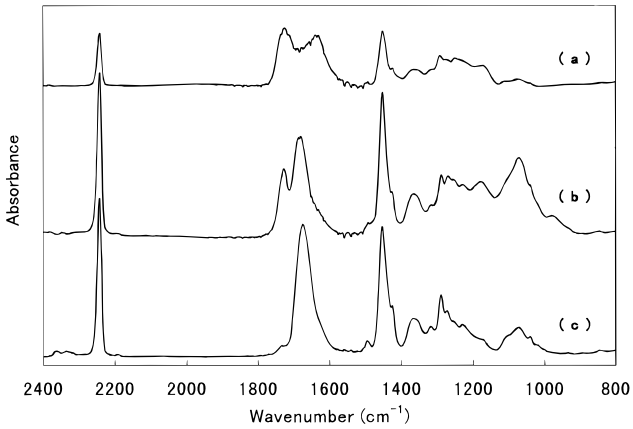

Figure 3. FT-IR/ATR spectra of PAN membrane surfaces grafted with anionic monomers: (a) AAc-*g*-PAN; (b) MOEP-*g*-PAN; (c) unmodified PAN.

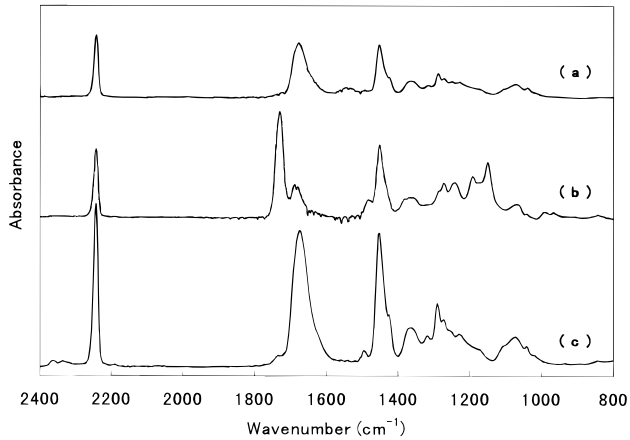

Figure 4. FT-IR/ATR spectra of PAN membrane surfaces grafted with cationic monomers: (a) DMAPAA-*g*-PAN; (b) DEAEM-*g*-PAN; (c) unmodified PAN.

polymerization, and "Unmodified PAN-2" was used as a control sample for comparison with the grafted PAN membranes. In heterogeneous graft polymerizations such as those we performed, detailed characterization of the graft chains within the pores is difficult due to the lack of analytical methods. We used the degree of reduction of pore diameter by AFM (see ref 34) and hydraulic permeability before and after the graft polymerization to prove that the amounts of MOEP and DEAEM grafted under these reaction conditions were larger than those of AAc and DMAPAA. These characteristics of the membranes can be reliable because the values are averaged over many data points. Furthermore, contact angle measurement[8,35] suggests that the MOEP-*g*-PAN and DEAEM-*g*-PAN surfaces were more hydrophobic than were those of AAc-*g*-PAN and DMAPAA-*g*-PAN.

3.2. FT-IR/ATR Characterization of Surface-Modified PAN Membranes. We performed FT-IR/ATR measurement, an effective method to characterize heterogeneously graft-polymerized surfaces, to confirm whether graft polymerization onto the PAN membranes was successfully achieved. Peaks were assigned by comparison of the IR spectra of the nominally grafted membranes with those of the unmodified PAN membrane (Unmodified PAN-1 in Table 1) and each pure anionic or cationic monomer (Figures 3 and 4, respectively), based on the literature.[36] Characteristics of the unmodified PAN membrane are strong absorption peaks

at 2243 cm^{-1} (C≡N), 1674 cm^{-1} (C═N), and 1454 cm^{-1} (CH_2) (Figure 3c or 4c). The valency bond vibration of oxime groups (C═N) at 1674 cm^{-1} is much stronger than that of the pure PAN powder we measured, showing that the oxime groups were formed while the dope solution was prepared. In the spectrum of the MOEP-*g*-PAN membrane (Figure 3b), the C═O stretching vibration of the ester groups at 1728 cm^{-1} adjacent to the C═N absorption band was newly developed. The bands at 1269 and 1178 cm^{-1} were developed from P═O and C−O (note that two kinds of stretching modes, i.e., C−O−(P) and C−O−(C), are included) stretching vibrations, respectively.[7,8,36] Also, the P−O−(H) and P−O−(C) stretching vibrations can be assigned at 980 and 1072 cm^{-1}, respectively.[7,8,36] The AAc-*g*-PAN membrane (Figure 3a) revealed a sharp peak at 1726 cm^{-1} arising from the C═O of the carboxylic acid groups in addition to that of the C═N groups. The C−O stretching vibration coupled with O−H in-plane bending can be observed at 1174 and 1252 cm^{-1}, resulting in enhancement of absorption in the range of 1100−1300 cm^{-1}.[37] The C═O (at 1730 cm^{-1}) and C−O (at 1192 cm^{-1}) stretching vibrations of the ester groups and the C−N stretching vibration of the tertiary amine groups (at 1151 cm^{-1}) can be clearly seen in the spectrum of the DEAEM-*g*-PAN membrane (Figure 4). The reaction conditions of the DMAPAA graft polymerization were poorer than those for the other samples; the only major visible difference in the spectrum of the resulting membrane from that of the unmodified PAN membrane was the newly developed peak at 1549 cm^{-1}, which can be assigned to the N−H deformational vibration of secondary amide groups. Other characteristic bands, for instance, the C═O vibration of the secondary amide groups and the C−N vibration of the tertiary amine groups, could not be identified in this spectrum. In the FT-IR/ATR spectra of the grafted PAN membranes, we observed some characteristic absorption bands from the graft chains in each sample. Although some degree of overlap among the characteristic bands and native PAN spectra complicated peak assignment, we confirmed the presence of the graft chains on the PAN membranes by comparison of the spectra before and after grafting. Note that these IR results provide information only of the surface and near surface of the membrane; the interior portions of the membrane, such as pore surfaces, cannot be characterized by this method.

3.3. ζ Potential of Unmodified and Grafted PAN Membranes. The Smoluchowski−Helmholtz equation, eq 1, and hence the Gouy−Chapman equation, eq 2, are valid only when $\kappa R \gg 1$, where R is the pore radius.[24,25,28] From AFM results, we estimate the pore diameters of the membranes analyzed in this study to have been ca. 50 nm (Table 1). Therefore, because κ^{-1} in the 1 mM KCl solution system corresponds to 10 nm, κR equals 2.5. However, since a wide distribution of pore diameter and surface roughness affect surface electrokinetic properties to a greater or lesser extent, conditions for application of the above equations to analysis of the pore surfaces in our membranes are, in fact, somewhat less than ideal.

The ζ potential of the unmodified PAN membranes as a function of hydraulic permeability, which may be proportional to pore diameter, remained unchanged over the range between 400 and 1200 $mL \cdot m^{-2} \cdot h^{-1} \cdot cm^{-1}$ H_2O (Figure 5). This suggests that a mean pore radius of ca. 25 nm is large enough for the Debye screening

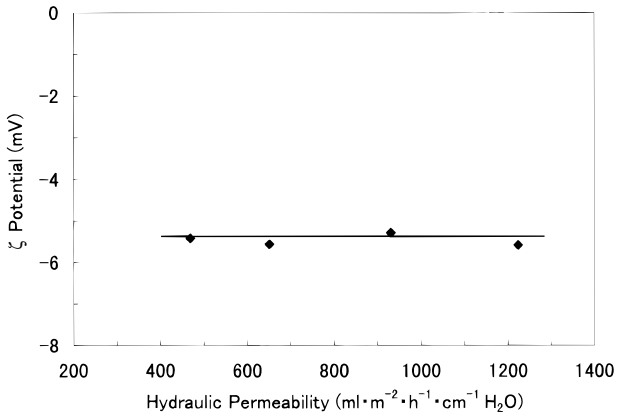

Figure 5. Variation in ζ potential of unmodified PAN membranes as a function of hydraulic permeability (1 mM KCl, pH 5.45).

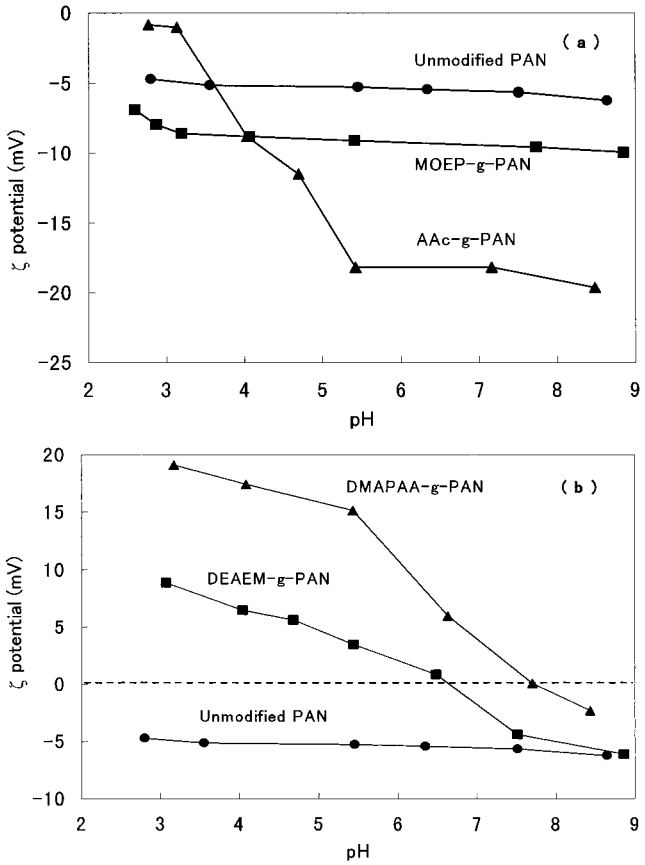

Figure 6. ζ potential variations in PAN membranes grafted with anionic (a) and cationic (b) monomers as a function of pH (1 mM KCl).

length, $\kappa^{-1} = 10$ nm, and sufficient for application of the Smoluchowski−Helmholtz equation. We considered relative values for the ζ potentials to be good enough for comparisons among different membranes with the same pore morphology, and thus we define ζ as an apparent value, as reported by Yan et al.[28]

The ζ potentials for the PAN membranes grafted with anionic and cationic monomers varied with pH (Figure 6). The ζ potential of the unmodified PAN membrane (corresponding to Unmodified PAN-2 in Table 1) was negative over the entire pH range, although this membrane has no charge groups. This result can be explained by specific adsorption of electrolyte anions onto the pore surfaces.[11,22,24] The ζ potentials of MOEP-*g*-

PAN and AAc-*g*-PAN membranes, with anionic groups, approached zero at low pH values. At higher pH values, the surface groups began to dissociate and the ζ potential increased until a plateau was reached; the ζ potential of the plateau depends on the number of dissociated groups.[30] In the case of the membranes with cationic charge groups, the ζ potential changed from negative to positive at an isoelectric point (iep) as pH decreased, in contrast to the patterns of the MOEP-*g*-PAN and AAc-*g*-PAN membranes. We attribute the negative values for the cationic membranes above the iep to specific adsorption of OH^-.[11] Though the degree of grafting of the MOEP-*g*-PAN and DEAEM-*g*-PAN was higher than that of the AAc-*g*-PAN and DMAPAA-*g*-PAN, we observed large differences in the maximum ζ potentials between MOEP-*g*-PAN and AAc-*g*-PAN, as well as between DEAEM-*g*-PAN and DMAPAA-*g*-PAN. These striking differences will be discussed below.

3.4. Surface Charge Density around the Pore Surface. Here we theoretically consider the above results based on a site dissociation model. When there is no specific adsorption of electrolyte ions, ionizable groups can contribute a surface charge. Equilibrium between charge groups and the solution at the interface is represented as

$$AH \leftrightarrow A^- + H^+ \tag{3}$$

$$B + H^+ \leftrightarrow BH^+ \tag{4}$$

where AH and B are acidic and basic groups, respectively. These equilibria are described with dissociation constants, K, as follows:

$$K_a = \frac{[A^-][H^+]_s}{[AH]} \tag{5}$$

$$K_b = \frac{[BH^+]}{[B][H^+]_s} \tag{6}$$

where subscripts a and b denote acid and base, respectively. $[H^+]_s$ is the hydronium ion concentration at the pore surface, which is assumed to follow the Boltzmann equation and is given by

$$[H^+]_s = [H^+]_0 \exp\left(\frac{-e\zeta}{2kT}\right) \tag{7}$$

where $[H^+]_0$ is the hydronium ion concentration in the bulk solution. The total site charge density of the pore surface, N, is described by

$$N_a = [A^-] + [AH] \tag{8}$$

$$N_b = [BH^+] + [B] \tag{9}$$

Thus, the surface charge density σ_s can be represented by combining eqs 5 and 6 with eqs 8 and 9, respectively, and one obtains

$$\sigma_{s,a} = -\left[\frac{eN_a}{1 + 10^{pK_a - pH_s}}\right] \quad \text{for an acidic site} \tag{10}$$

$$\sigma_{s,b} = \left[\frac{eN_b}{1 + 10^{pH_s - pK_b}}\right] \quad \text{for a basic site} \tag{11}$$

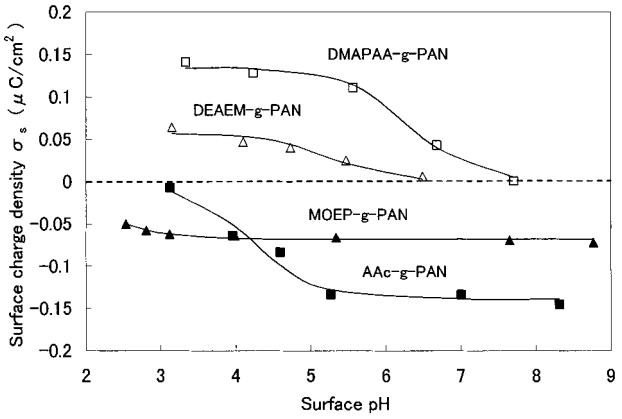

Figure 7. Variations in surface charge density for grafted PAN membranes as a function of surface pH. Drawn lines correspond to theoretical fits using a single site dissociation model.

Table 2. Characteristic Parameters for Pore Surface of Grafted PAN Membranes Derived from the Site Dissociation Model

sample	pK_a	pK_b	$10^3 N_a$ (nm^{-2})	$10^3 N_b$ (nm^{-2})
MOEP-*g*-PAN	2.1		4.25	
AAc-*g*-PAN	4.2		8.67	
DEAEM-*g*-PAN		5.3		3.57
DMAPAA-*g*-PAN		6.3		8.37

where pK_a and pK_b are the acidic and basic equilibrium site dissociation constants, respectively, and pH_s is the surface pH. The surface charge density σ_s was calculated from the ζ potential using eq 2 and plotted as a function of surface pH (calculated from eq 7) in Figure 7. Table 2 lists the parameters derived from the curve fits using eqs 10 and 11 on a site dissociation model in Figure 7. The grafted membranes show characteristic surface pK values for the dissociation of the charge groups. The large differences in the maximum ζ potential and the corresponding site charge density, N, between MOEP-*g*-PAN and AAc-*g*-PAN, as well as between DEAEM-*g*-PAN and DMAPAA-*g*-PAN (see Figure 6 and Table 2) will be explained on the basis of both the configuration model of the graft chains[7,11] and ion-pairing effects.[32]

3.5. Configuration Model for Effective Surface Charge Density. Uchida et al.[11] suggested that ζ potential variation as a function of molecular weight of graft chains that reveals poor water solubility can be explained by a configuration model of the graft chains. Graft chain length depends on the magnitude of the ζ potential in which the grafted surface shows either hydrophobicity or hydrophilicity. According to the model,[7,11] short graft chains are in a soluble state in water so that many charge groups can contribute to the surface charge. Relatively long graft chains overspread the surface and are precipitated to become hydrophobic surfaces because of poor solubility in water. As a consequence, the dissociation of the charge groups may be suppressed by high concentrations of graft chains, and thus only a small proportion of the charge groups contribute to the surface charge. Applying this concept to our present study, the membrane surfaces having poly(AAc) and poly(DMAPAA) chains are more hydrophilic than those having poly(MOEP) and poly(DEAEM) chains, as can be demonstrated by the fact that the contact angles of AAc-*g*-poly(ethylene) and DMAPAA-*g*-poly(ethylene terephthalate) are much lower than

those of MOEP-*g*-poly(ethylene) and DMAEMA-*g*-poly(ethylene terephthalate), respectively; in both cases the differences in the contact angles are about 20 deg when the graft density exceeds 1.5 μg·cm^{-2}.[7,8,35] We assumed that the contact angle behavior of poly(DEAEM) used in this study nearly corresponds to that of poly((dimethylamino)ethyl methacrylate) (poly(DMAEMA)).[35] Thus, the graft chains of AAc-*g*-PAN and DMAPAA-*g*-PAN are in a more water-soluble state in an aqueous medium. Further, as previously mentioned, there is evidence that the MOEP-*g*-PAN and DEAEM-*g*-PAN membranes were grafted much more than the AAc-*g*-PAN and DMAPAA-*g*-PAN membranes, respectively. Thus the large differences in the maximum ζ potentials and the site charge densities, N_a, between AAc-*g*-PAN and MOEP-*g*-PAN membranes (see Figure 6 and Table 2, respectively) may arise from different proportions of the charge groups contributing to the surface charge; the dissociation of the surface charge groups of the more hydrophobic MOEP-*g*-PAN membrane seems to be more suppressed by the high concentrations of the graft chains than is that of the AAc-*g*-PAN membrane. The same phenomenon can also be observed in the case of DMAPAA-*g*-PAN and DEAEM-*g*-PAN membranes. Confidence in this explanation, however, is limited by a poor theoretical background.

3.6. Ion-Pairing Effect for Effective Surface Charge Density. Before we discuss the ion-pairing effects of the membrane surface charge, the following must be noted. Bearing eq 1 in mind, the bulk dielectric constant ϵ and viscosity η are used for the electrical double layer. Lyklema and Overbeek have justified the use of the bulk ϵ value without any corrections in the Smoluchowski−Helmholtz equation for electrophoretic mobility under conditions of low potential and low ionic strength.[38] On the other hand, the solution viscosity is influenced by the increase in surface potential and electrolyte concentration.[38] However, in our applied measurement system, the surface potential and electrolyte concentration were low enough that the change in viscosity would be negligible. We do not need to incorporate any errors with respect to ϵ and η to apply the Smoluchowski−Helmholtz equation (eq 1), and further distinguish the bulk ϵ from the local dielectric constant ϵ_1 that is assumed in evaluation of the ion-pairing effect.

The model we introduce to explain the results from the ζ potential measurement was suggested by Mafé et al.[32] for a charged membrane on the basis of the effects of ion-pair formation between the membrane fixed charge groups and counterions. The effective charge density of a charged membrane with low water content depends on such ion-pairing effects. On the other hand, Saito et al.[39] have shown that the effective charge density of highly swollen poly(vinyl alcohol) membranes decreases as the degree of hydration increases. This result can be explained by a three-phase model that consists of three states of electrolyte ions in the membrane. However, note that their study is based on membranes with high water content. In our study, although the membrane pores are completely filled with aqueous solution, the grafted chain phase located at the interface between the membrane support and aqueous solution phases can be considered to have had a low water content, particularly for the hydrophobic graft chains. Therefore, the ion-pairing effects model is very useful for explaining both the states of the pore surface charge as well as the so-called effective charge concentration of ion-exchange membranes. This model will be applicable not only to membrane systems with low water content but also to those with high water content. Some of the charge groups within membranes with hydrophobic matrix polymers cannot be hydrated because they are less accessible to water molecules; some of the counterions then form ion pairs with the membrane fixed-charge groups (schematically shown in Figure 1 in ref 32). Mafé et al.[32] have theoretically analyzed the effective charge fraction, the activity coefficient and the co-ion concentration within charged membranes as a function of the ratio of the concentration of the external solution to that of the fixed charge, by incorporating ion-pairing effects. Considering the above, the local dielectric constant surrounding ion pairs should facilitate understanding of our ζ potential measurement results. The detailed description of the ion-pairing model we used is shown in refs 32, 40, and 41.

We define the total membrane charge concentration $X \equiv X_f + X_b$ where X_f is the concentration of free membrane charge groups and X_b is the concentration of the membrane charge groups that form ion pairs. According to the Fuoss approach, an ion pair's association constant can be written on the basis of the linear Poisson−Boltzmann equation as[40]

$$K_A = (4\pi 10^{-24} N_A/3)(a/\mathrm{nm})^3 \exp(b) \qquad (12)$$

$$b \equiv \frac{e^2}{4\pi\epsilon_1\epsilon_0 a k T}$$

where N_A is Avogadro's number, e the Coulombic charge, ϵ_1 the local dielectric constant in a pair (note that ϵ_1 is distinguished from ϵ in eq 1), k the Boltzmann constant, and a the center-to-center distance between the ions in a pair. Introducing $\Phi \equiv X_f/X$ as a fraction of the free fixed-charge groups, the following equation can then be obtained from the ideal Donnan equation and the Fuoss approach, in addition to some corrections with the Debye−Hückel activity coefficient for nondilute electrolyte solutions and the entropy change due to ion-pairing formation.[32]

$$(4\pi 10^{-24} N_A/3)(a/\mathrm{nm})^3 \exp\left[\frac{b}{1+\kappa a} - 3\ln\frac{(1/(XN_A))^{1/3}}{2a}\right] = \frac{1-\Phi}{\Phi\{(\Phi X/2) + [(\Phi X/2)^2 + c_s^{\,2}]^{1/2}\}} \qquad (13)$$

$$b \equiv \frac{e^2}{4\pi\epsilon_1\epsilon_0 a k T}$$

$$\kappa^{-1} \equiv \left\{\frac{\epsilon_1\epsilon_0 R T}{2F^2[(\Phi X/2)^2 + c_s^{\,2}]^{1/2}}\right\}^{1/2}$$

where κ^{-1} is the Debye−Hückel length, R the gas constant, c_s the concentration of the uni-univalent electrolyte solution, and F the Faraday constant. We consider the correlation between the free fixed-charge fraction Φ and the local dielectric constant ϵ_1 using eq 13. Some characteristic parameters were introduced to the model calculations: $a = 4.0$ Å, $\epsilon_1 = 5 - 13$, and $X = 2 \times 10^{-4} - 2 \times 10^{-2}$ M.[32]

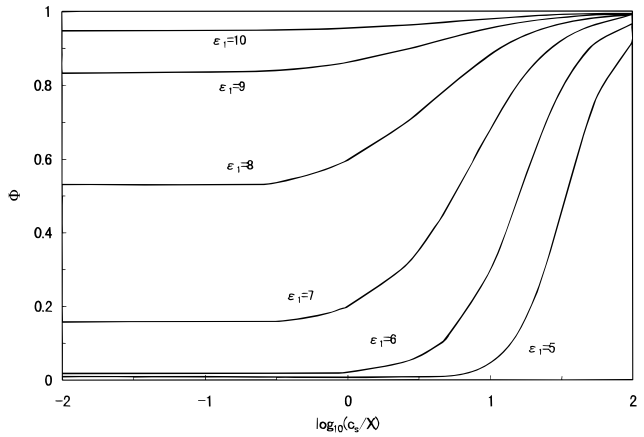

Figure 8. Variations in free fixed-charge fraction Φ as a function of $\log(c_s/X)$ with various local dielectric constants ($X = 2 \times 10^{-3}$ M, $a = 4.0$ Å).

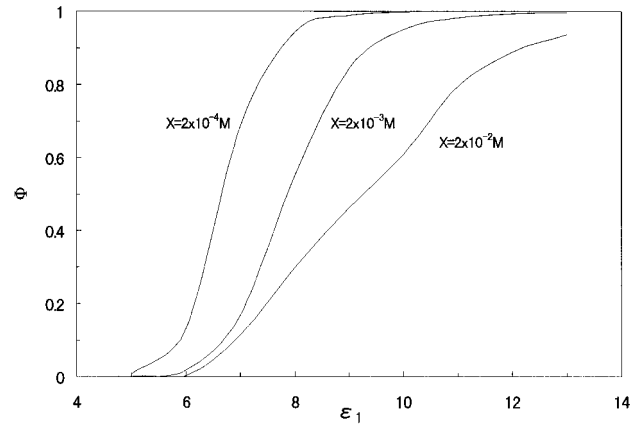

Figure 9. Variations in free fixed-charge fraction Φ as a function of local dielectric constant ϵ_1 with various concentrations of fixed charge groups ($c_s = 1 \times 10^{-3}$ M, $a = 4.0$ Å).

Figure 8 shows the variations in Φ as a function of $\log(c_s/X)$ with various ϵ_1 values as calculated with eq 13. For a specified value of X (2×10^{-3} M), Φ increased with increasing concentration of the external solution c_s and increased remarkably at low dielectric constants less than 8; this result implies that Φ depends significantly on c_s and ϵ_1. The higher ϵ_1 values, which correspond to a more hydrophilic environment, lead to less ion pair formation. Figure 9 shows the dependence of Φ relative to the variation in the local dielectric constant ϵ_1 for three kinds of fixed charge concentrations at $c_s = 1 \times 10^{-3}$ M. The calculated curves reveal that Φ approaches unity asymptotically with a sigmoidal shape as ϵ_1 increases, and thus Φ depends strongly on the magnitude of ϵ_1. The threshold of an abrupt increase in Φ shifts to a lower value of ϵ_1 with decreasing X. From the above theoretical simulations, it can be concluded that the free fixed-charge fraction Φ depends significantly on the local dielectric constant ϵ_1.

The local dielectric constants of hydrophobic charged surfaces are lower than those of hydrophilic surfaces, affecting ion-pair formation. Although the MOEP-*g*-PAN and DEAEM-*g*-PAN membranes were grafted much more than the AAc-*g*-PAN and DMAPAA-*g*-PAN membranes, respectively, the maximum ζ potential and the site charge density of the former are much smaller than those of the latter. Moreover, the former is more hydrophobic than the latter, as mentioned above. In these respects, this result can be explained by a significant difference in the local dielectric constant between them; the charge groups of the hydrophobic membranes are more likely to form ion pairs with counterions than are those of the hydrophilic membranes, thus leading to a suppression of dissociation of the charge groups. Also, the hydrophilic membranes are highly hydrated, and hence their local dielectric constants might be high enough for ion-pairing effects to decay. The maximum ζ potential and site charge density will differ significantly between hydrophobic and hydrophilic surfaces because local dielectric constant influences ion-pair formation. From the above results, we conclude that this model considering ion-pairing effects provides a more reasonable explanation of the differences in the surface charge states between hydrophobic and hydrophilic membranes than do configuration models of graft chains.

4. Conclusions

The top surface of grafted PAN membranes was analyzed by AFM and FT-IR/ATR to confirm graft polymerization. ζ potential measurement proved to be a novel and useful method for characterizing the pore surface properties of such membranes. However, because ζ potential depends largely on the pore diameter and surface roughness, large differences in these factors make comparison between samples impossible, even on a relative scale. If one can prepare well-defined membranes, the results from ζ potential measurement can be evaluated according to a single site dissociation model for pH dependence, which provides much information on the pore surface properties pK, iep, and charge density. Application of this model to membrane systems greatly facilitates not only characterization of surface modification but also interpretation of such complicated phenomena as membrane−protein interaction. The large charge state differences between the hydrophobic and hydrophilic surfaces we observed can be better explained by ion-pairing effects than by configuration models of the graft chains, for which the dissociation of the charge groups is suppressed for the hydrophobic surfaces. This suppression of dissociation can be successfully shown by the relationship between the local dielectric constant and the effective fixed-charge concentration. The states of surface charge groups, therefore, seem to depend greatly on the local dielectric constant surrounding ion pairs.

Acknowledgment. We express our great appreciation to Dr. Seiji Hayashi and Mr. Jun Okumura (Mitsubishi Rayon Co., Ltd., Japan) for kindly providing poly(acrylonitrile) powder. We would also like to thank Dr. Xu Weigang for experimental support in the FT-IR/ATR analyses and Dr. Tatsuji Murata for AFM images.

References and Notes

(1) Bamford, C. H.; Al−Lamee, K. G. *Polymer* **1994**, *35*, 2844.
(2) Bamford, C. H.; Al−Lamee, K. G. *Polymer* **1996**, *37*, 4885.
(3) Ulbricht, M.; Oechel, A.; Lehmann, C.; Tomaschewski, G.; Hicke, H.-G. *J. Appl. Polym. Sci.* **1995**, *55*, 1707.
(4) Ulbricht, M.; Matushewski, H.; Oechel, A.; Hicke, H.-G. *J. Membr. Sci.* **1996**, *115*, 31.
(5) Godjevargova, T.; Dimov, A. *J. Membr. Sci.* **1992**, *67*, 283.
(6) Godjevargova, Z.; Dimov, A.; Petrov, S. *J. Appl. Polym. Sci.* **1992**, *44*, 2139.
(7) Tretinnikov, O. N.; Ikada, Y. *Macromolecules* **1997**, *30*, 1086.
(8) Tretinnikov, O. N.; Kato, K.; Ikada, Y. *J. Biomed. Mater. Res.* **1994**, *28*, 1365.

(9) Iwata H. *J. Appl. Polym. Sci.* **1994**, *52*, 445.
(10) Lai, J. Y.; Tseng, C. W.; Lee, K. R. *J. Appl. Polym. Sci.* **1996**, *61*, 307.
(11) Uchida, E.; Uyama, Y.; Ikada, Y. *Langmuir* **1994**, *10*, 1193.
(12) Ter-Minassian-Saraga, L. *J. Colloid Interface Sci.* **1981**, *80*, 393.
(13) Noinville, V.; Vidal-Madjar, C.; Sébille, B. *J. Phys. Chem.* **1995**, *99*, 1516.
(14) Ramsden, J. J.; Prenosil, J. E. *J. Phys. Chem.* **1994**, *98*, 5376.
(15) Absolom, D. R.; Zingg, W.; Neumann, A. W. *J. Biomed. Mater. Res.* **1987**, *21*, 161.
(16) Ikada, Y. *Adv. Polym. Sci.* **1984**, *57*, 103.
(17) Miller, M. L. *Can. J. Chem.* **1958**, *36*, 303.
(18) Bajaj, P.; Chavan, R. B.; Manjeet, B. *J. Macromol. Sci., Chem.* **1985**, *A22*, 1219.
(19) Simitzis, J. *Acta Polym.* **1994**, *45*, 104.
(20) Jacobasch, H. J.; Schurz, J. *Prog. Colloid Polym. Sci.* **1988**, *77*, 40.
(21) Ribitsch, V.; Jorde, C.; Schurz, J.; Jacobasch, H. J. *Prog. Colloid Polym. Sci.* **1988**, *77*, 49.
(22) Werner, C.; Jacobasch, H. J.; Reichelt, G. *J. Biomater. Sci., Polym. Ed.* **1995**, *7*, 61.
(23) Cohen Stuart, M. A.; Tamai, H. *Macromolecules* **1988**, *21*, 1863.
(24) Causserand, C.; Nyström, M.; Aimar, P. *J. Membr. Sci.* **1994**, *88*, 211.
(25) Nyström, M.; Pihlajamäki, A.; Ehsani, N. *J. Membr. Sci.* **1994**, *87*, 245.
(26) Burns, N. L.; Holmberg, K.; Brink, C. *J. Colloid Interface Sci.* **1996**, *178*, 116.
(27) Burns, N. L.; Van Alstine, J. M.; Harris, J. M. *Langmuir* **1995**, *11*, 2768.
(28) Yan, F.; Déjardin, P.; Schmitt, A.; Pusineri, C. *J. Phys. Chem.* **1993**, *97*, 3824.
(29) Scales, P. J.; Grieser, F.; Healy, T. W.; White, L. R.; Chan, D. Y. C. *Langmuir* **1992**, *8*, 965.
(30) Marlow, B. J.; Rowell, R. L. *Langmuir* **1991**, *7*, 2970.
(31) Healy, T. W.; White, L. R. *Adv. Colloid Interface Sci.* **1978**, *9*, 303.
(32) Mafé, S.; Ramírez, P.; Tanioka, A.; Pellicer, J. *J. Phys. Chem. B* **1997**, *101*, 1851.
(33) Hernández, A.; Martínez, F.; Martín, A.; Prádanos, P. *J. Colloid Interface Sci.* **1995**, *173*, 284.
(34) Fretzsche, A. K.; Arevalo, A. R.; Moor, M. D.; O′Hara, C. *J. Membr. Sci.* **1993**, *81*, 109.
(35) Uchida, E.; Uyama, Y.; Ikada. Y. *J. Appl. Polym. Sci.* **1993**, *47*, 417.
(36) Bellamy, L. J. In *The Infrared Spectra of Complex Molecules*; Wiley: New York, 1975.
(37) Dong, J.; Ozaki, Y.; Nakashima, K. *Macromolecules* **1997**, *30*, 1111.
(38) Lyklema, J.; Overbeek, J. T. G. *J. Colloid Sci.* **1961**, *16*, 501.
(39) Saito, K.; Tanioka, A.; Miyasaka, K. *Polymer* **1994**, *35*, 5098.
(40) Fuoss, R. M. *J. Am. Chem. Soc.* **1958**, *80*, 5059.
(41) Bockris, J. O′M.; Reddy, A. K. N. In *Modern Electrochemistry*; Plenum: New York, 1970; Chapter 3.

MA970692K